Locally-Optimal Electric Sail Transfer

Proc IMechE Part G:
J Aerospace Engineering
2019, Vol. 233(1) 166–179
IMechE 2017

DOI:10.1177/0954410017728975
journals.sagepub.com/home/pig

Marco Bassetto, **Alessandro A. Quarta*** and **Giovanni Mengali**
Department of Civil and Industrial Engineering, University of Pisa, I-56122 Pisa, Italy

Abstract

This paper analyzes the locally-optimal heliocentric transfer of a spacecraft propelled by an Electric Solar Wind Sail, an innovative propellantless propulsion system that generates a propulsive acceleration exploiting the momentum of solar wind particles. The potentialities of such an advanced thruster are investigated in terms of flight times required to achieve a given heliocentric orbit. The problem is addressed using a locally optimal formulation, by minimizing a scalar performance index that depends on the time derivatives of the osculating orbital elements. The proposed algorithm gives an estimate of the globally optimal flight time with reduced computational efforts compared to a traditional optimization approach. Also, when the performance index involves a single orbital parameter and the transfer trajectory is two-dimensional, the proposed approach provides an analytical solution to the locally-optimal control problem. The procedure discussed in the paper is used to quantify the near-optimal performance of an Electric Solar Wind Sail in some advanced mission scenarios, such as the design of a heliocentric non-Keplerian orbit for solar activity monitoring, the exploration of the Solar System boundaries, and the rendezvous with comets 1P Halley and 67P/Churyumov-Gerasimenko.

Keywords

Electric Solar Wind Sail, locally-optimal control laws, non-singular orbital elements, mission analysis, interplanetary trajectories

Nomenclature

$\mathbb{A}$	=	state matrix
$\boldsymbol{a}$	=	propulsive acceleration [$\mathrm{mm/s^2}$]
a	=	semimajor axis [au]
a_c	=	characteristic acceleration [$\mathrm{mm/s^2}$]
a_n	=	normal component of $\boldsymbol{a}$ [$\mathrm{mm/s^2}$]
a_r	=	radial component of $\boldsymbol{a}$ [$\mathrm{mm/s^2}$]

* Corresponding author; e-mail: a.quarta@ing.unipi.it

a_t = tangential component of $\boldsymbol{a}$ [$\mathrm{mm/s^2}$]
$b_a, b_e, b_i, b_\Omega, b_\omega$ = dimensionless scalar weights
$\boldsymbol{c}$ = vector, see Eq. (4)
e = orbital eccentricity
$\hat{\boldsymbol{e}}_r, \hat{\boldsymbol{e}}_t, \hat{\boldsymbol{e}}_n$ = unit vectors of RTN reference frame
$\boldsymbol{h}$ = specific angular momentum vector [$\mathrm{km^2/s}$]
i = orbital inclination [rad]
J = performance index
$k_{\text{œ}}$ = auxiliary function
L = true longitude [rad]
$\hat{\boldsymbol{n}}$ = unit vector normal to the E-sail nominal plane
œ = generic orbital element
p, f, g, h, k, L = modified equinoctial orbital elements
R, d = dimensionless constants, see Eq. (22)
$\boldsymbol{r}$ = position vector, with $r = \|\boldsymbol{r}\|$ [au]
$r_\oplus$ = reference distance (1 au)
S = spacecraft center-of-mass
t = time [days]
u = argument of latitude [rad]
$\boldsymbol{x}$ = state vector
α = cone angle [rad]
α_n = pitch angle [rad]
γ = dimensionless propulsive acceleration modulus
δ = clock angle [rad]
$\mu_\odot$ = Sun's gravitational parameter [$\mathrm{km^3/s^2}$]
ν = true anomaly [rad]
τ = switching variable
ϕ = phasing angle [rad]
Ω = right ascension of the ascending node [rad]
ω = argument of perihelion [rad]

Subscripts

0 = initial
f = final
max = maximum, aphelion
min = minimum, perihelion

Superscripts

$\star$ = locally-optimal
$\cdot$ = time derivative
$\wedge$ = unit vector
$\sim$ = reduced

1. Introduction

The optimal transfer between two heliocentric orbits using a reaction engine usually consists in finding the trajectory that minimizes a linear combination of the total velocity variation and the flight time [1,2]. Due to the finite amount of available propellant, the use of reaction engines limits the spacecraft maneuvering capabilities to such an extent that they may become ineffective when the target orbit is considerably different from the initial one. In this context, the use of propellantless, continuous-thrust propulsion systems represents a fascinating and interesting option [3], especially when either high-energy transfers are sought, or long-term deep space missions must be accomplished without the need of complex gravity assist maneuvers.

This paper investigates the potentialities of the Electric Solar Wind Sail (E-sail) for different mission scenarios based on locally-optimal control laws. The latter are obtained by minimizing the instantaneous variation of a suitable combination of osculating orbital elements related to the characteristics of both the parking and target orbits [4]. The results associated to locally-optimal trajectories can be used as a starting guess for a succeeding analysis of globally optimal trajectories, in which, for example, an approach based on the classical calculus of variations [5] or on direct optimization algorithms [6] is used to find the minimum flight time. Unlike most of the existing results on E-sail mission design, which are obtained with a simplified thrust model [5,7], this paper uses the most recent E-sail thrust mathematical model [8,9,10] that accounts for a dependence of both the modulus and direction of the thrust vector on the spacecraft attitude.

2. Mathematical model

Consider an E-sail-based spacecraft that covers a heliocentric parking orbit of given characteristics. The spacecraft is modelled as a point mass subjected to the gravitational force of the Sun and to the E-sail propulsive acceleration. The spacecraft state is defined by a set of non-singular Modified Equinoctial Orbital Elements [11,12] (MEOEs) $\{p,\, f,\, g,\, h,\, k,\, L\}$, which are related to the classical orbital elements $\{a,\, e,\, i,\, \Omega,\, \omega,\, \nu\}$ of the osculating orbit by the following relationships:

$$p = a\left(1-e^2\right) \quad , \quad f = e\cos(\Omega+\omega) \quad , \quad g = e\sin(\Omega+\omega) \quad ,$$
$$h = \tan(i/2)\cos\Omega \quad , \quad k = \tan(i/2)\sin\Omega \quad , \quad L = \nu+\Omega+\omega \qquad (1)$$

where a is the semimajor axis, e is the orbital eccentricity, i is the orbital inclination, Ω is the right ascension of the ascending node, ω is the argument of perihelion, and ν is the true anomaly. The spacecraft heliocentric motion is described through the vectorial differential equation [13]

$$\dot{\boldsymbol{x}} = \mathbb{A}\,\boldsymbol{a} + \boldsymbol{c} \qquad (2)$$

where $\boldsymbol{x} \triangleq [p,\, f,\, g,\, h,\, k,\, L]^{\mathrm{T}}$ is the state vector, matrix $\mathbb{A} \in \mathbb{R}^{6\times 3}$ is defined as

$$\mathbb{A} \triangleq \sqrt{\frac{p}{\mu_{\odot}}} \begin{bmatrix} 0 & \dfrac{p}{1+f\,\cos L+g\,\sin L} & 0 \\ \sin L & \dfrac{(2+f\,\cos L+g\,\sin L)\,\cos L+f}{1+f\,\cos L+g\,\sin L} & -\dfrac{g\,(h\,\sin L-k\,\cos L)}{1+f\,\cos L+g\,\sin L} \\ -\cos L & \dfrac{(2+f\,\cos L+g\,\sin L)\,\sin L+g}{1+f\,\cos L+g\,\sin L} & \dfrac{f\,(h\,\sin L-k\,\cos L)}{1+f\,\cos L+g\,\sin L} \\ 0 & 0 & \dfrac{(1+h^2+k^2)\,\cos L}{2\,(1+f\,\cos L+g\,\sin L)} \\ 0 & 0 & \dfrac{(1+h^2+k^2)\,\sin L}{2\,(1+f\,\cos L+g\,\sin L)} \\ 0 & 0 & \dfrac{h\,\sin L-k\,\cos L}{1+f\,\cos L+g\,\sin L} \end{bmatrix} \tag{3}$$

and vector $\boldsymbol{c} \in \mathbb{R}^{6\times 1}$ is

$$\boldsymbol{c} \triangleq \sqrt{\mu_{\odot}\,p}\left(\frac{1+f\,\cos L+g\,\sin L}{p}\right)^{2}\,[0,\,0,\,0,\,0,\,0,\,1]^{\mathrm{T}} \tag{4}$$

where $\mu_{\odot}$ is the Sun's gravitational parameter. Note that Eq. (2) is free from singularities, since $(1+f\,\cos L+g\,\sin L) \equiv p/r > 0$, being r the Sun-spacecraft distance and p the semilatus rectum of the spacecraft osculating orbit. In Eq. (2), $\boldsymbol{a}$ is the spacecraft propulsive acceleration vector, whose components are written in a radial-tangential-normal orbital reference frame $\mathcal{T}_{\mathrm{RTN}}(S;\,\hat{\boldsymbol{e}}_r,\,\hat{\boldsymbol{e}}_t,\,\hat{\boldsymbol{e}}_n)$, see Fig. 1, whose unit vectors are

$$\hat{\boldsymbol{e}}_r \triangleq \boldsymbol{r}/\|\boldsymbol{r}\| \quad , \quad \hat{\boldsymbol{e}}_n \triangleq \boldsymbol{h}/\|\boldsymbol{h}\| \quad , \quad \hat{\boldsymbol{e}}_t \triangleq \hat{\boldsymbol{e}}_n \times \hat{\boldsymbol{e}}_r \tag{5}$$

where $\boldsymbol{r}$ is the Sun-spacecraft vector, and $\boldsymbol{h}$ is the spacecraft specific angular momentum vector. In Fig 1, $\hat{\boldsymbol{n}}$ is the unit vector perpendicular to the E-sail nominal plane in the direction opposite to the Sun. Note that $\boldsymbol{a}$ belongs to the plane $(\hat{\boldsymbol{e}}_r,\,\hat{\boldsymbol{n}})$ if $\hat{\boldsymbol{e}}_r \neq \hat{\boldsymbol{n}}$, whereas $\hat{\boldsymbol{a}} \equiv \hat{\boldsymbol{e}}_r$ if $\hat{\boldsymbol{n}} \equiv \hat{\boldsymbol{e}}_r$.

Taking into account the recent numerical simulations by Yamaguchi and Yamakawa [8,9], the components of vector $\boldsymbol{a}$ in $\mathcal{T}_{\mathrm{RTN}}$ are

$$[\boldsymbol{a}]_{\mathcal{T}_{\mathrm{RTN}}} \triangleq [a_r,\,a_t,\,a_n]^{\mathrm{T}} = a_c\,\tau\left(\frac{r_{\oplus}}{r}\right)\gamma\,[\cos\alpha, \quad -\sin\alpha\,\sin\delta, \quad \sin\alpha\,\cos\delta]^{\mathrm{T}} \tag{6}$$

where a_c is the spacecraft characteristic acceleration (i.e. the maximum value of $\|\boldsymbol{a}\|$ at a Sun-spacecraft reference distance $r_{\oplus} \triangleq 1\,\mathrm{au}$), $\tau \in \{0,\,1\}$ is the switching variable that models the thruster on/off modes, and $\gamma \in (0,\,1]$ is the dimensionless propulsive acceleration modulus, defined as the ratio of the local value of $\|\boldsymbol{a}\|$ at a given E-sail attitude to the local maximum propulsive acceleration modulus $\|\boldsymbol{a}\|_{\max}$. In Eq. (6), α is the cone angle, that is, the angle between the Sun-spacecraft line and the direction of the propulsive acceleration vector $\boldsymbol{a}$, and $\delta \in [0,\,2\pi]\,\mathrm{rad}$ is the clock angle, defined as the angle (measured counterclockwise) between the direction of $\boldsymbol{h}$ and the projection of $\hat{\boldsymbol{n}}$ on the local horizontal plane (i.e. the plane perpendicular to the Sun-spacecraft line), see Fig. 1. Note that the values of both γ and α are functions of the sail pitch angle $\alpha_n \in [0,\,\alpha_{n_{\max}}]\,\mathrm{rad}$, see Fig. 2, the latter being the angle between $\hat{\boldsymbol{e}}_r$ and $\hat{\boldsymbol{n}}$. The value of the maximum pitch angle is taken equal to $\alpha_{n_{\max}} \triangleq \pi/3\,\mathrm{rad}$, in order to prevent the E-sail from possible mechanical instabilities [10]. Accordingly, the three spacecraft scalar control variables are $\{\alpha_n,\,\delta,\,\tau\}$.

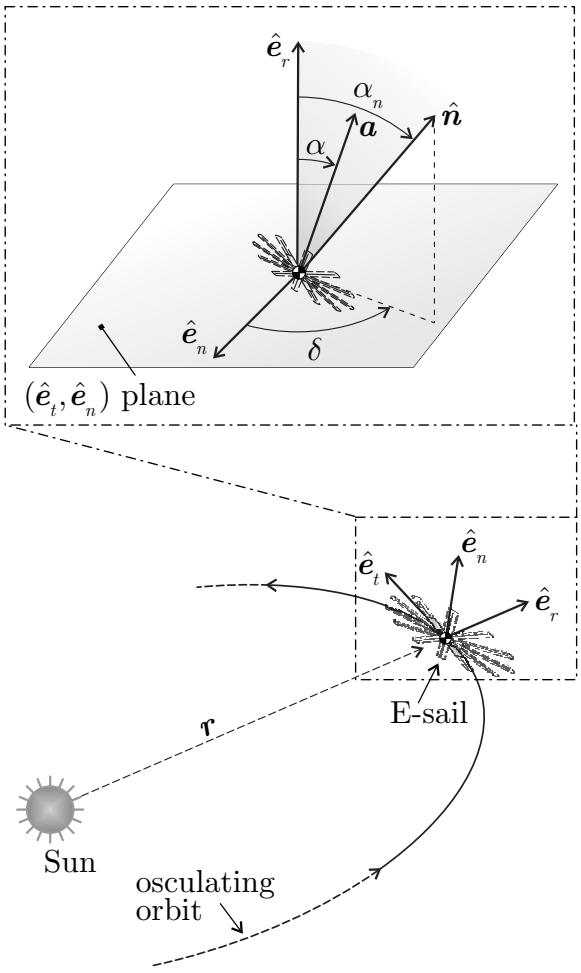

Figure 1. Reference frame and E-sail characteristic angles.

2.1. Locally-optimal control laws

The problem addressed in this paper is to find the control laws $\alpha_n = \alpha_n(t)$, $\delta = \delta(t)$, and $\tau = \tau(t)$ that minimize, at any time, the functional J defined by a linear combination of the time derivatives of the osculating orbital elements, viz.

$$J = b_a \frac{\mathrm{d}(a/a_0)}{\mathrm{d}t} + b_e \frac{\mathrm{d}e}{\mathrm{d}t} + b_i \frac{\mathrm{d}i}{\mathrm{d}t} + b_\Omega \frac{\mathrm{d}\Omega}{\mathrm{d}t} + b_\omega \frac{\mathrm{d}\omega}{\mathrm{d}t} \tag{7}$$

where a_0 is the parking orbit semimajor axis, and $\{b_a, b_e, b_i, b_\Omega, b_\omega\}$ are dimensionless scalar weights. The structure of J is very general and is useful for dealing with problems where a simultaneous control of different orbital elements is required. In general, only a subset of the scalar weights is chosen to be different from zero. This choice depends on the type of problem to be studied, as is better described in the succeeding mission examples. In particular, when J contains more than a single term in the summation, each scalar weight is selected through a trial-and-error approach.

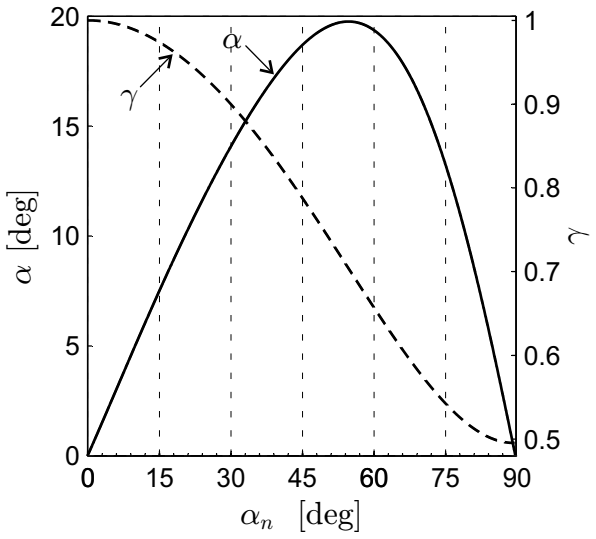

Figure 2. Cone angle α and dimensionless propulsive acceleration γ as a function of pitch angle α_n, see also Fig. 1. Figure adapted from Ref. [10]

To proceed, recall that the time derivatives of the osculating orbital elements are given by [14]

$$\frac{\mathrm{d}a}{\mathrm{d}t} = 2\sqrt{\frac{a^3}{\mu_\odot\,(1-e^2)}}\,\left[e\,\sin\nu\,a_r + (1+e\,\cos\nu)\,a_t\right] \tag{8}$$

$$\frac{\mathrm{d}e}{\mathrm{d}t} = \sqrt{\frac{a\,(1-e^2)}{\mu_\odot}}\,\left[\sin\nu\,a_r + \left(\cos\nu + \frac{e+\cos\nu}{1+e\,\cos\nu}\right)\,a_t\right] \tag{9}$$

$$\frac{\mathrm{d}i}{\mathrm{d}t} = \sqrt{\frac{a\,(1-e^2)}{\mu_\odot}}\,\frac{\cos u}{1+e\,\cos\nu}\,a_n \tag{10}$$

$$\frac{\mathrm{d}\Omega}{\mathrm{d}t} = \sqrt{\frac{a\,(1-e^2)}{\mu_\odot}}\,\frac{\sin u}{(1+e\,\cos\nu)\,\sin i}\,a_n \tag{11}$$

$$\frac{\mathrm{d}\omega}{\mathrm{d}t} = \sqrt{\frac{a\,(1-e^2)}{\mu_\odot}}\,\left[-\frac{\cos\nu}{e}\,a_r + \frac{2+e\,\cos\nu}{e\,(1+e\,\cos\nu)}\,\sin\nu\,a_t - \frac{\sin u\,\cot i}{1+e\,\cos\nu}\,a_n\right] \tag{12}$$

where $u = \omega + \nu$ is the argument of latitude. These expressions are functions of the classical orbital parameters. However, recalling that

$$a = \frac{p}{1-f^2-g^2} \quad , \quad e = \sqrt{f^2+g^2} \quad , \quad i = 2\arctan\sqrt{h^2+k^2} \quad ,$$
$$\tan\Omega = \frac{k}{h} \quad , \quad \tan\omega = \frac{g\,h - f\,k}{f\,h + g\,k} \quad , \quad \nu = L - \Omega - \omega \tag{13}$$

it is possible to obtain a set of time derivatives of the osculating orbital elements in terms of MEOEs. The result is

$$\frac{\mathrm{d}a}{\mathrm{d}t} = \frac{\dot{p}\,\left(1-f^2-g^2\right)+2\,p\,(f\,\dot{f}+g\,\dot{g})}{\left(1-f^2-g^2\right)^2} \tag{14}$$

$$\frac{\mathrm{d}e}{\mathrm{d}t} = \frac{f\,\dot{f}+g\,\dot{g}}{\sqrt{f^2+g^2}} \tag{15}$$

$$\frac{\mathrm{d}i}{\mathrm{d}t} = \frac{2\,(h\,\dot{h}+k\,\dot{k})}{\left(1+h^2+k^2\right)\,\sqrt{h^2+k^2}} \tag{16}$$

$$\frac{\mathrm{d}\Omega}{\mathrm{d}t} = \frac{\dot{k}\,h-k\,\dot{h}}{k^2+h^2} \tag{17}$$

$$\frac{\mathrm{d}\omega}{\mathrm{d}t} = \frac{(\dot{g}\,h+g\,\dot{h}-\dot{f}\,k-f\,\dot{k})\,(f\,h+g\,k)+(\dot{f}\,h+f\,\dot{h}+\dot{g}\,k+g\,\dot{k})\,(f\,k-g\,h)}{1+\left(f\,k-g\,h\right)^2} \tag{18}$$

$$\frac{\mathrm{d}\nu}{\mathrm{d}t} = \dot{L}-\dot{\Omega}-\dot{\omega} \tag{19}$$

where $\{\dot{p},\,\dot{f},\,\dot{g},\,\dot{h},\,\dot{k},\,\dot{L}\}$ are functions of the control variables $\{\alpha_n,\,\delta,\,\tau\}$ through Eqs. (2) and (6).

Returning to Eq. (7), it may be easily checked that J is a linear function of τ. Accordingly, the minimum value of J can be found with the following two-step procedure. First, using the Nelder-Mead simplex method [15], the ratio J/τ is numerically minimized with respect to $\{\alpha_n,\,\delta\}$ by looking for the optimal control angles $\alpha_n^\star$ and $\delta^\star$. Then, the optimal switching variable $\tau^\star$ is obtained from

$$\tau^\star = \frac{1-\mathrm{sign}\left(\tilde{J}\right)}{2} \qquad \text{with} \qquad \tilde{J} \triangleq \frac{J\,(\alpha_n=\alpha_n^\star,\,\delta=\delta^\star)}{\tau} \tag{20}$$

where $\mathrm{sign}\,(\cdot)$ is the signum function.

In some cases the propulsive acceleration vector $\boldsymbol{a}$ is constrained to belong to the osculating orbital plane ($a_n=0$), or to the $(\hat{\boldsymbol{e}}_r,\,\hat{\boldsymbol{e}}_n)$ plane ($a_t=0$). When $a_n=0$ (or $a_t=0$), the clock angle can take only two values, that is, $\delta=\{\pi/2\,,\,3\pi/2\}\,\mathrm{rad}$ (or $\delta=\{0,\,\pi\}\,\mathrm{rad}$). In those cases, δ may be removed from the set of control variables, assuming $\alpha_n\in[-\alpha_{n_{\max}}\,,\,\alpha_{n_{\max}}]$, with the additional condition $\mathrm{sign}\,(\alpha_n)=\mathrm{sign}\,(\boldsymbol{a}\cdot\hat{\boldsymbol{e}}_t)$ if $a_n=0$, or $\mathrm{sign}\,(\alpha_n)=\mathrm{sign}\,(\boldsymbol{a}\cdot\hat{\boldsymbol{e}}_n)$ if $a_t=0$.

When the optimization process involves a single orbital element $\mathrm{o\!e}\in\{a,\,e,\,i,\,\Omega,\,\omega,\,\nu\}$, the locally-optimal value $\alpha_n^\star$ of the E-sail pitch angle can be analytically found by enforcing the necessary condition

$$\frac{\partial}{\partial\alpha_n}\left(\frac{\mathrm{d}\mathrm{o\!e}}{\mathrm{d}t}\right)=0 \tag{21}$$

where the generic time derivative $\mathrm{d}\mathrm{o\!e}/\mathrm{d}t$ is obtained from Eqs. (8)–(12). According to Fig. 2, and bearing in mind the analytical approximations of the functions $\alpha=\alpha\,(\alpha_n)$ and $\gamma=\gamma\,(\alpha_n)$ given by [10]

$$\alpha=\arctan\left[\frac{R\,\sin\left(2\,\alpha_n\right)}{d+R\,\cos\left(2\,\alpha_n\right)}\right] \quad , \quad \gamma=\sqrt{d^2+R^2+2\,R\,d\,\cos\left(2\,\alpha_n\right)} \tag{22}$$

with $R \triangleq 0.2523$ and $d \triangleq 0.7477$, the solutions $\{\alpha_{n_1}, \alpha_{n_2}\}$ of Eq. (21) for the generic orbital element œ can be written in a compact form as

$$\alpha_{n_1} = \arcsin\left(\sqrt{\frac{k_{œ}^2 - k_{œ}\sqrt{k_{œ}^2+1}+1}{2\,(k_{œ}^2+1)}}\right) \tag{23}$$

$$\alpha_{n_2} = \alpha_{n_1} - \frac{\pi}{2} \tag{24}$$

where $k_{œ}$ depends on the specific orbital element to be optimized, viz.

$$k_a = \frac{e\,\sin\nu}{1+e\,\cos\nu} \tag{25}$$

$$k_e = \frac{\sin\nu\,(1+e\,\cos\nu)}{e\,\cos^2\nu + 2\,\cos\nu + e} \tag{26}$$

$$k_\omega = -\frac{(1+e\,\cos\nu)\,\cos\nu}{(2+e\,\cos\nu)\,\sin\nu} \tag{27}$$

$$k_i \equiv k_\Omega = 0 \tag{28}$$

Even though $\{\alpha_{n_1}, \alpha_{n_2}\}$ are functions of e and ν only, the locally-optimal value $\alpha_n = \alpha_n^\star(t)$ must account for the sign of the time derivatives of the orbital elements, which are also functions of the argument of latitude u, see Eqs. (10)–(12). The results are summarized in graphical form in Figs. 3–7, where the eccentricity is chosen within the interval $e \in [0.1,\, 0.9]$, corresponding to closed osculating orbits. Note, however, that Eqs. (23)–(28) are valid for any value of the orbital eccentricity.

From Fig. 3, the semimajor axis can always be increased (or decreased) when $\nu \in [0,\, \pi]$ rad ($\nu \in [\pi,\, 2\pi]$ rad), independently of the osculating orbital eccentricity. This same conclusion does not apply beyond those intervals of true anomaly, when the eccentricity exceeds a limiting value of about 0.3374. For example, if the osculating orbital eccentricity is 0.4, the time variation of a is negative for all values of α_n if $\nu \in [217.8,\, 282.8]$ deg, see Fig. 3(a).

Figure 4 shows that it is not possible to optimize the orbital eccentricity for any value of the true anomaly. In particular, the interval in which a local maximization (minimization) cannot be achieved is slightly dependent on the osculating orbital eccentricity. For example, a maximization of e is not possible when $\nu \in [215.0,\, 323.8]$ deg if $e = 0.1$, while the interval of "forbidden" true anomalies is $[202.5,\, 320.8]$ deg if $e = 0.9$. Note that Figs. 3(a)–3(b) and Figs. 4(a)–4(b) are symmetric to each other with respect to the point $[180,\, 0]$ on the $(\nu,\, \alpha_n^\star)$ plane.

Likewise, the local optimization of the argument of perihelion is not possible for all values of ν, see Fig. 5. In particular, from Fig. 5(a) an increase of ω cannot be achieved around the perihelion, while Fig. 5(b) suggests that a reduction of the argument of perihelion is not possible when the E-sail flies close to the osculating aphelion. More precisely, ω cannot be increased (decreased) when $\nu \in [-55.1,\, 55.1]$ deg if $e = 0.1$ ($\nu \in [126.5,\, 233.5]$ deg), while the intervals of forbidden true anomalies are $\nu \in [-58.9,\, 58.9]$ deg and $\nu \in [126.5,\, 233.5]$ deg, respectively, if $e = 0.9$. Figure 5(b) points out that the optimum pitch angle to minimize ω slightly depends on the osculating eccentricity.

The pitch angles for the optimization of i and Ω do not depend on e, but are functions of the argument of latitude u, see Figs. 6–7. In addition, i and Ω can always be increased (or decreased) for any value of u.

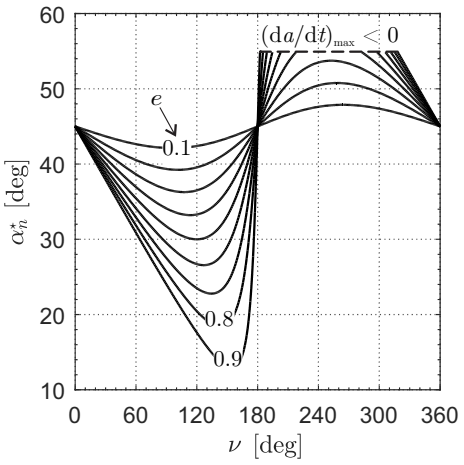

(a) Maximization of $\mathrm{d}a/\mathrm{d}t$

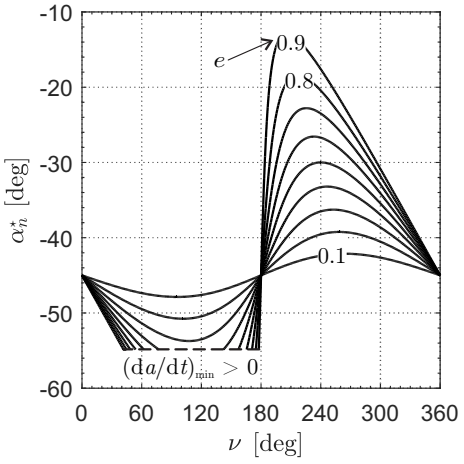

(b) Minimization of $\mathrm{d}a/\mathrm{d}t$

Figure 3. Value of pitch angle $\alpha_n^\star$, as a function of $\{e, \nu\}$, for optimization of $\mathrm{d}a/\mathrm{d}t$.

3. Mission applications

The locally-optimal steering laws in analytical form are an useful tool in the analysis of some advanced mission scenarios, including the case of rotation of the apse line (optimization of $\mathrm{d}\omega/\mathrm{d}t$), the outer Solar System exploration (maximization of $\mathrm{d}a/\mathrm{d}t$), and the cranking maneuver of a heliocentric orbit (optimization of $\mathrm{d}i/\mathrm{d}t$). The typical approach to the analysis of such mission scenarios consists in determining the trajectory that minimizes the total flight time, or minimizes the characteristic acceleration necessary for a given mission duration. However, a globally-optimal approach requires a significant computational effort and an initial estimate of the solution, independently of the mission profile to be analyzed.

In this sense, when compared to a global optimization approach, the use of a locally-optimal method provides a substantial simplification of the mathematical problem and guarantees a considerable reduction of the computational costs. To better emphasize the performance of a locally-optimal control law, some exemplary mission cases will now be discussed in detail.

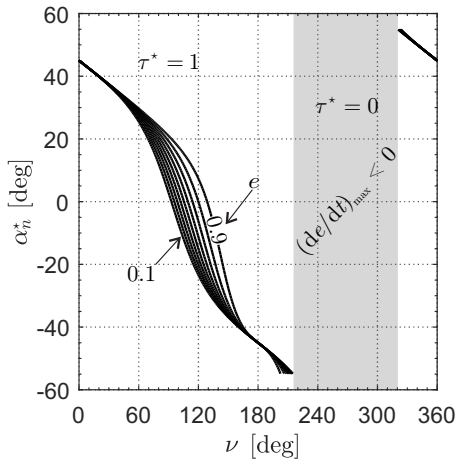

(a) Maximization of $\mathrm{d}e/\mathrm{d}t$

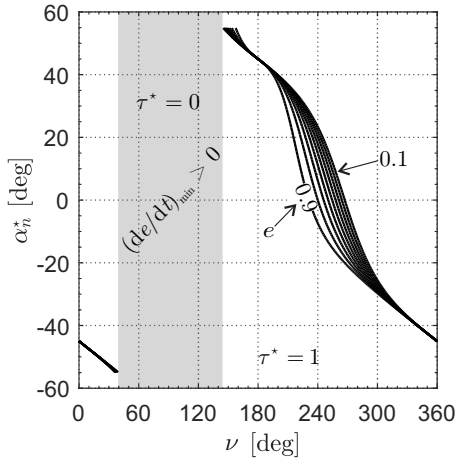

(b) Minimization of $\mathrm{d}e/\mathrm{d}t$

Figure 4. Value of pitch angle $\alpha_n^\star$, as a function of $\{e, \nu\}$, for optimization of $\mathrm{d}e/\mathrm{d}t$.

3.1. Earth-following orbits

In this case, the apse line of the spacecraft osculating orbit follows the Earth in its heliocentric motion (a so called Earth-Following Orbit, EFO). According to Heiligers and McInnes [16], such an orbit is useful, for example, for solar activity monitoring and Near-Earth-Object surveillance. The basic idea is to place the spacecraft into an eccentric orbit belonging to the ecliptic plane, whose apse line precedes at a mean angular rate $\overline{\dot{\omega}} \triangleq 2\pi\,\mathrm{rad/\,year}$. This amounts to having a phasing angle ϕ between the osculating orbit apse line and the Sun-Earth vector, see Fig. 8, which fluctuates in time with zero mean value. Assuming an initial spacecraft position at $\nu = 0$ (with the perihelion in opposition to the Earth), the locally-optimal control law is chosen to minimize the performance index $J = -\mathrm{d}\omega/\mathrm{d}t$, see Eq. (7) in which $b_\omega = -1$ and $b_a = b_e = b_i = b_\Omega = 0$. For a given characteristic acceleration, the semimajor axis and eccentricity of the parking orbit are then chosen such that the constraint $\overline{\dot{\omega}} \triangleq 2\pi\,\mathrm{rad/\,year}$ is met.

Since the spacecraft motion takes place on the ecliptic plane, the normal component of the propulsive acceleration is $a_n = 0$. The equations of motion (2) are numerically integrated with a pitch angle $\alpha_n^\star = \alpha_{n_1}$ (or $\alpha_n^\star = \alpha_{n_2}$) if $\nu \in [0,\, \pi]\,\mathrm{rad}$ (or $\nu \in [\pi,\, 2\pi]\,\mathrm{rad}$) where $\{\alpha_{n_1},\, \alpha_{n_2}\}$ are given by Eqs. (23)-(24) with $k_{\text{œ}} = k_\omega$

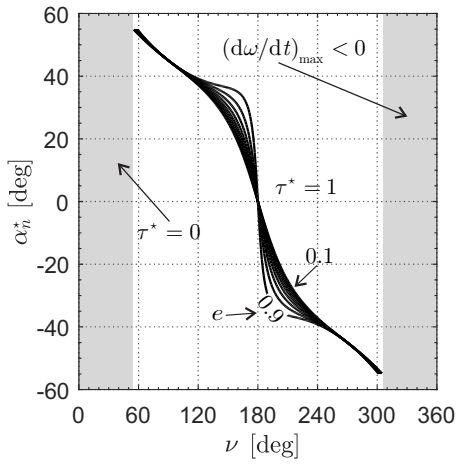

(a) Maximization of $\mathrm{d}\omega/\mathrm{d}t$

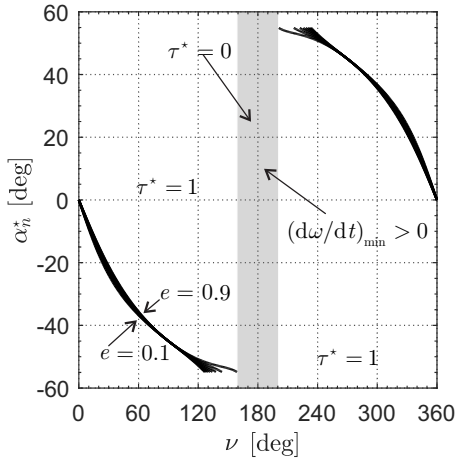

(b) Minimization of $\mathrm{d}\omega/\mathrm{d}t$

Figure 5. Value of pitch angle $\alpha_n^\star$, as a function of $\{e, \nu\}$, for optimization of $\mathrm{d}\omega/\mathrm{d}t$ with $a_n = 0$.

and k_ω taken from Eq. (27), see also Fig. 5(a). In this case the locally-optimal switching variable $\tau^\star$ is given by Eq. (20) where $\mathrm{sign}\left(\tilde{J}\right) \equiv \mathrm{sign}\left(-\dot{\omega}\left(\alpha_n = \alpha_n^\star\right)\right)$.

Figure 9(a) shows the possible pairs $\{a_0, e_0\}$ of initial orbital elements that solve the problem for a given value of $a_c \in [0.25, 1.5]\,\mathrm{mm/s^2}$, i.e. for a medium-low performance E-sail. Not all the pairs $\{a_0, e_0\}$ turn out to be admissible and, in fact, the forbidden region on the right hand side of Fig. 9(a) corresponds to initial conditions that provide an insufficient apsidal precession rate, while the dotted line defines the constraint about the minimum heliocentric distance, set equal to 0.25 au, which is introduced to prevent the E-sail from an excessive thermal load [7]. The possible combinations of aphelion ($r_{\max}$) and perihelion ($r_{\min}$) distances as functions of the parking orbit characteristics $\{a_0, e_0\}$ are shown in Fig. 9(b).

For example, consider a spacecraft trajectory with a perihelion radius $r_{\min} = 0.4\,\mathrm{au}$ and an aphelion radius $r_{\max} = 0.6\,\mathrm{au}$. According to Fig. 9(a), the parking orbit characteristics are $a_0 \simeq 0.42\,\mathrm{au}$ and $e_0 \simeq 0.06$, while the required characteristic acceleration is $a_c \simeq 1\,\mathrm{mm/s^2}$. Figure 10(a) shows the time-variation of the locally-optimal steering law $\{\alpha_n^\star(t), \tau^\star(t)\}$, whereas Figs. 10(b)-10(c) show the time-variation of semimajor axis a and eccentricity e of the spacecraft osculating orbit. Note that the functions $a = a\,(t)$ and $e = e\,(t)$ are periodic with the same frequency, as they take their initial values at the end of each on/off cycle. The periodicity of a and e

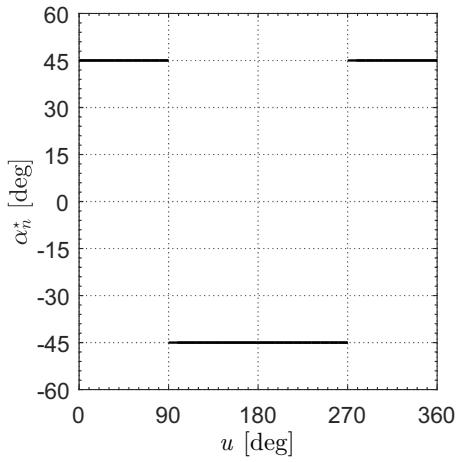

(a) Maximization of $\mathrm{d}i/\mathrm{d}t$

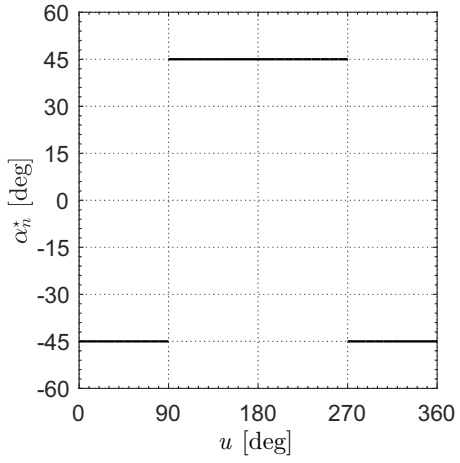

(b) Minimization of $\mathrm{d}i/\mathrm{d}t$

Figure 6. Value of pitch angle $\alpha_n^\star$, as a function of $u = \nu + \omega$, for optimization of $\mathrm{d}i/\mathrm{d}t$.

occurs for any combination of initial conditions $\{a_0, e_0\}$ and E-sail characteristic acceleration a_c. The oscillation period of a and e can only be calculated numerically, and depends on a_c and on the orbital elements of the parking orbit (a_0 and e_0).

The spacecraft trajectory is illustrated in Fig. 11(a) for a flight time of 2 years, while Fig. 11(b) shows the time variation of angle ϕ, see Fig. 8. As expected, the mean value of the phasing angle ϕ is zero, whereas its maximum amplitude $|\phi_{\max}|$ is about 17 deg. Similar to the oscillation period of a and e, the value of $|\phi_{\max}|$ depends on the characteristics of the parking orbit $\{a_0, e_0\}$ and on the performance of the E-sail through its characteristic acceleration. Within the chosen interval of a_c, the simulations show that $|\phi_{\max}|$ is always below 23.5 deg, see Fig. 12. In the limiting case as a_c tends to zero (spacecraft Keplerian orbit), the apse line does not rotate at all ($\omega \equiv \omega_0$) and $|\phi_{\max}|$ tends to 180 deg.

3.2. Outer Solar System exploration

The study of the Heliosheath, a region approximatively located at a distance of about 100 au from the Sun, and the interstellar medium is a fundamental issue for an in-depth analysis of the Solar System evolution. Currently, the farthermost artificial object from the Sun is the Voyager 1 probe, which was launched in 1977 and is now

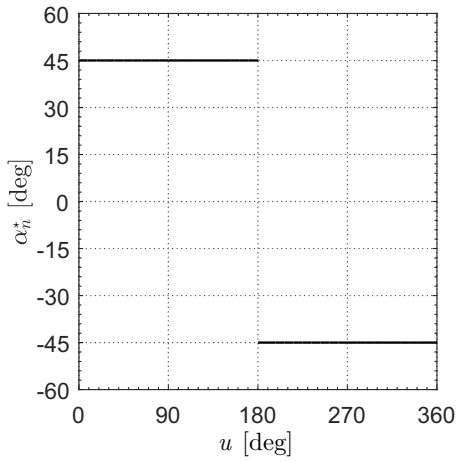

(a) Maximization of $\mathrm{d}\Omega/\mathrm{d}t$

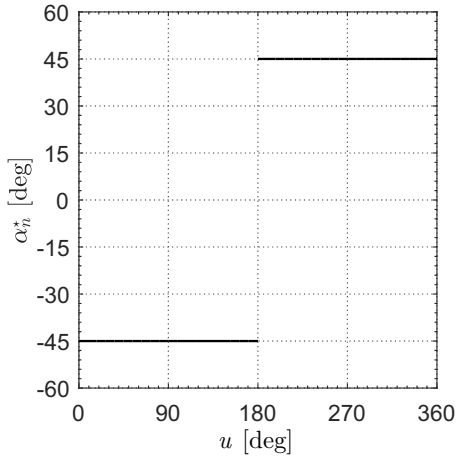

(b) Minimization of $\mathrm{d}\Omega/\mathrm{d}t$

Figure 7. Value of pitch angle $\alpha_n^\star$, as a function of $u = \nu + \omega$, for optimization of $\mathrm{d}\Omega/\mathrm{d}t$.

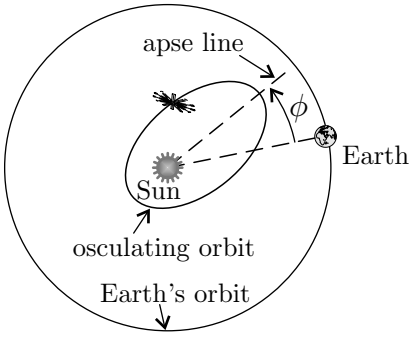

Figure 8. Phasing angle ϕ in an Earth-following orbit.

travelling at a heliocentric distance[1] of about 140 au, with a cruise speed [17] of 17 km/s (roughly corresponding to 3.6 au/year).

[1] Data retrieved (July 19, 2017) from official Voyager 1 website at `https://voyager.jpl.nasa.gov/where/`

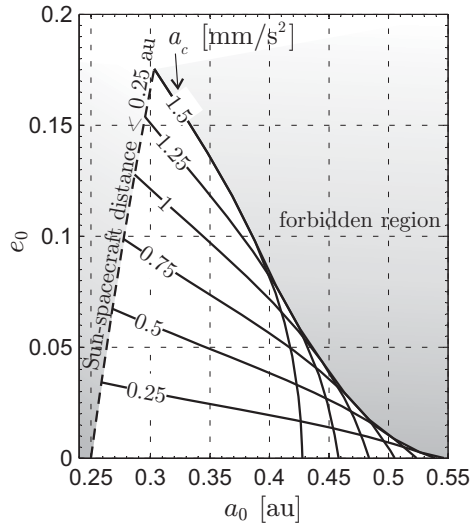

(a) Parking orbit characteristics.

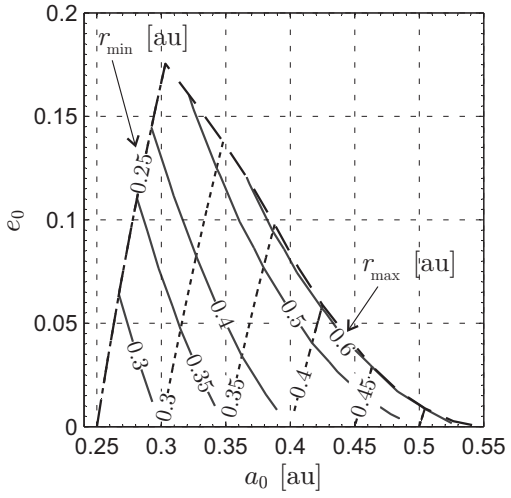

(b) Perihelion ($r_{\min}$) and aphelion ($r_{\max}$) distance.

Figure 9. Parking orbits characteristics and Sun-spacecraft extreme distances for an EFO with a medium-low performance E-sail.

The locally-optimal control laws can be used to evaluate the near-minimum flight time required for a spacecraft to reach a given distance r_f with $e_f \geq 1$. The results are obtained using medium-high performance E-sails, with a characteristic acceleration $a_c \in [1,\, 2]\,\mathrm{mm/s^2}$ and a circular (heliocentric) parking orbit of radius $r_0 = 1\,\mathrm{au}$. The locally-optimal control law minimizes $-\dot{a}$ (that is, $b_a = -1$ and $b_e = b_i = b_\omega = b_\Omega = 0$ in Eq. (7)), which amounts to maximizing the time variation of the specific mechanical energy. In this case, the optimum pitch angle $\alpha_n^\star$ is given by Eq. (23), where $k_\text{œ} = k_a$, and k_a is defined in Eq. (25) as a function of $\{e,\, \nu\}$. The switching variable $\tau^\star$ is given by Eq. (20), where $\mathrm{sign}\left(\tilde{J}\right) = \mathrm{sign}\left(-\dot{a}\,(\alpha_n = \alpha_n^\star)\right)$.

The total flight time t_f and the hyperbolic excess speed v_∞ are shown in Fig. 13 as a function of the final heliocentric distance $r_f \leq 100\,\mathrm{au}$ and for different values of the spacecraft characteristic acceleration a_c. For each value of a_c, the maximum r_f is consistent with the Sun-Heliosheath distance, whereas the minimum r_f corresponds to an insertion of the spacecraft into a parabolic orbit ($e_f = 1$) with a transfer trajectory shown in Fig. 14. In particular, Fig. 13(a) shows that a flight time of about 23 years is required to reach the Heliosheath

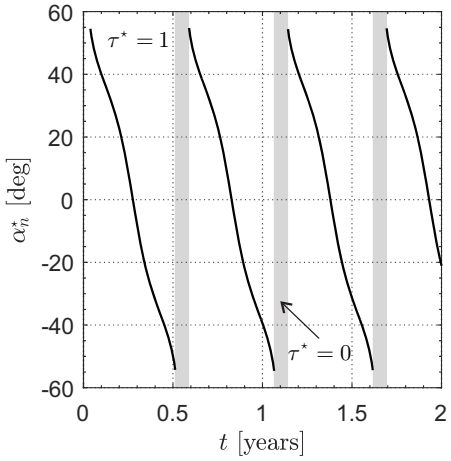

(a) Pitch angle and switching variable.

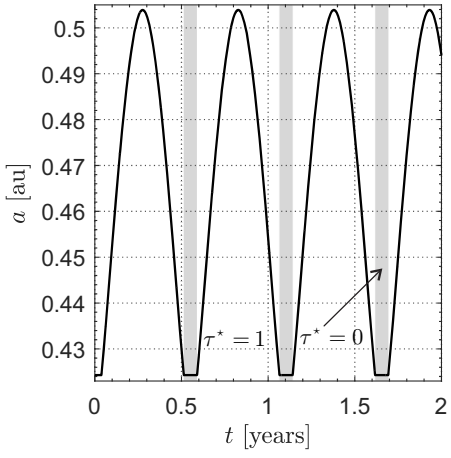

(b) Osculating orbit semimajor axis.

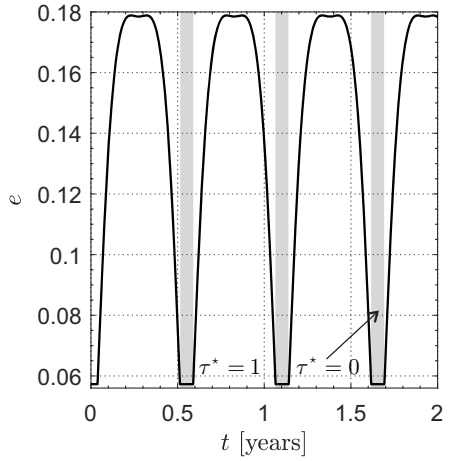

(c) Osculating orbit eccentricity.

Figure 10. Time variation of the locally-optimal control law and osculating orbit characteristics for an EFO with $a_c = 1\text{mm/s}^2$, $r_{\min} = 0.4\text{au}$ and $r_{\max} = 0.6\text{au}$.

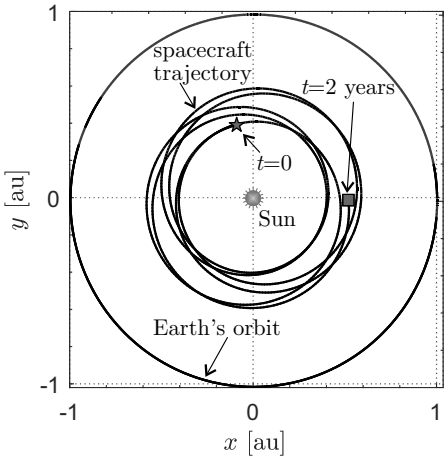

(a) Spacecraft trajectory in the Ecliptic plane.

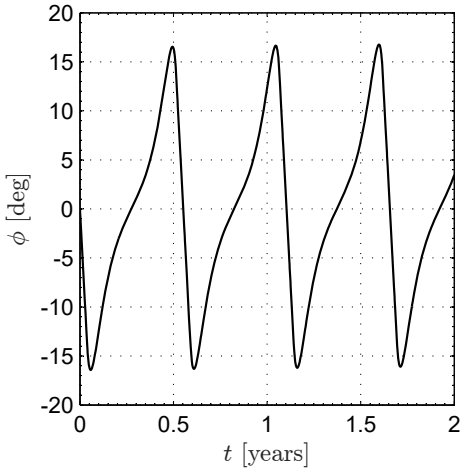

(b) Phase displacement ϕ.

Figure 11. Locally-optimal EFO with $a_c = 1\text{mm/s}^2$, $r_{\min} = 0.4\text{au}$ and $r_{\max} = 0.6\text{au}$.

with $a_c = 1\,\text{mm/s}^2$, while it is roughly halved when the characteristic acceleration is doubled. Figure 13(b) shows the spacecraft hyperbolic excess speed as a function of r_f and a_c. Note that, in the worst considered case of $a_c = 1\,\text{mm/s}^2$, a hyperbolic excess speed grater than 3.6 au/year (about the same of Voyager 1) is reached with a flight time of about 8 years. Note that the behaviour of the functions $t_f = t_f(a_c, r_f)$ and $v_\infty = v_\infty(a_c, r_f)$ are consistent with those discussed by Quarta and Mengali [7] in a similar mission scenario. In particular, employing the previous E-sail thrust model [5,18], Ref. [7] uses a global optimization method (based on an indirect approach) to evaluate the minimum time trajectory for a transfer to the Solar System boundaries.

Assuming, for example, $r_f = 100\,\text{au}$ and $a_c = \{1, 2\}\,\text{mm/s}^2$, Fig. 15 shows the time variation of the pitch angle $\alpha_n^\star$, while the locally-optimal switching variable is always $\tau^\star = 1$ since the spacecraft osculating true anomaly belongs to $[0, \pi]$ rad during the whole transfer, see Fig. 3(a).

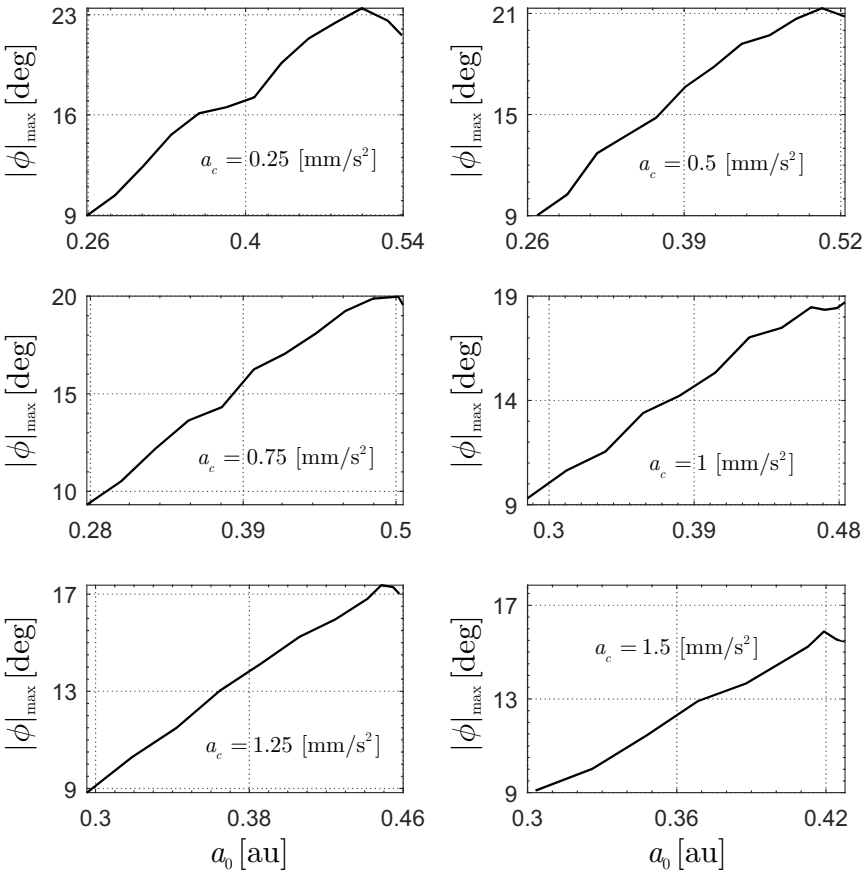

Figure 12. Maximum phasing angle $|\phi|_{\max}$ as function of parking orbit characteristics $\{a_0, e_0\}$ and $a_c \in [0.25, 1.5]\text{mm/s}^2$.

3.3. Rendezvous with Comet 1P/Halley

Comet 1P/Halley is the most famous and brilliant comet of the Kuiper belt, and a transfer trajectory toward this fascinating celestial body with an E-sail-based spacecraft is a challenging test case, as its retrograde orbit is characterized by high values of orbital eccentricity. In this case the spacecraft parking orbit is assumed to coincide with the Earth's heliocentric orbit, while the orbital elements of Comet Halley are evaluated through an ephemeris calculation. The E-sail characteristic acceleration is set equal to $1\,\text{mm/s}^2$, and a minimum heliocentric distance constraint of 0.25 au has been enforced. This kind of orbital transfer is difficult to obtain with a conventional propulsion system due to the high amount of propellant it requires.

The whole transfer has been conceptually divided into three phases, as is shown in Fig. 16. In each phase the solution has been obtained by minimizing the time variation of a different linear combination of the osculating orbital elements, see Eq. (7). A numerical integration of Eqs. (2) is made for each mission phase, with initial conditions corresponding to the final conditions of the preceding integration.

During the first phase of the transfer, the spacecraft reduces its distance from the Sun in order to increase the E-sail thrust maximum modulus. This can be obtained by minimizing a linear combination of $\dot{a}$ and $\dot{e}$. After a two-year long transfer, the spacecraft reaches a near-circular orbit with a semimajor axis of 0.25 au, see Fig. 16(a). Then, the spacecraft performs a cranking maneuver during which it maintains a nearly constant distance from the Sun, until the orbital inclination and the right ascension of the ascending node meet those of Halley's heliocentric orbit, see Fig. 16(b). In this second phase the control law minimizes a linear combination

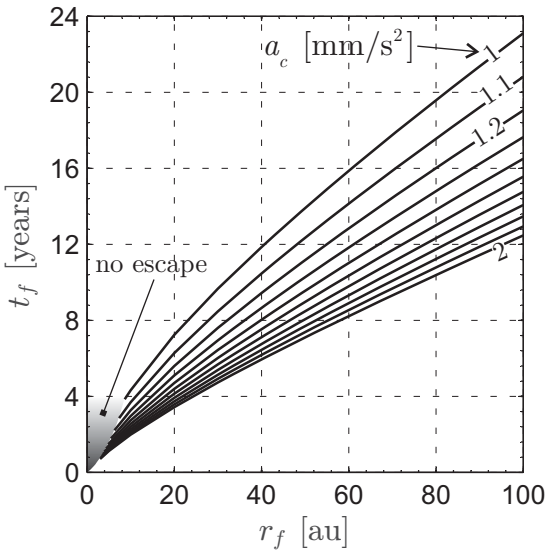

(a) Flight time.

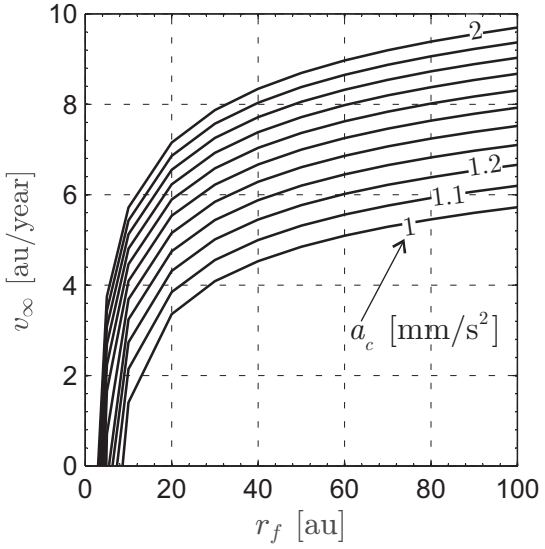

(b) Hyperbolic excess speed.

Figure 13. Near-optimal performance to reach a given Sun-spacecraft distance r_f as a function of a_c.

of the time derivatives of i and Ω. At the end of the second phase, about 11 years from the beginning of the transfer, the semimajor axis and the eccentricity are 0.25 au and 0.02, respectively. In the last phase the orbital radius is increased, while maintaining the orbital inclination and the value of Ω unchanged, until the cometary rendezvous, see Fig. 16(c). In this phase, the corresponding locally-optimal control law linearly combines $\dot{a}$, $\dot{e}$ and $\dot{\omega}$.

Table 1 summarizes the parking orbit conditions [19] and the orbital parameters at the end of each phase. The cometary rendezvous occurs when the celestial body true anomaly is equal to 138 deg and the heliocentric distance is about 4.13 au. The transfer data are summarized in Tab. 1. Given the total flight time, it is found that the spacecraft leaves the parking orbit on the 24$^{\text{th}}$ of June 2046 and meets the comet on the 3$^{\text{rd}}$ of May 2062. The near-optimal flight time is less than 16 years, which is a good result taking into account the characteristics of the comet's orbit (retrograde and highly eccentric) and recalling that the whole transfer is accomplished with no

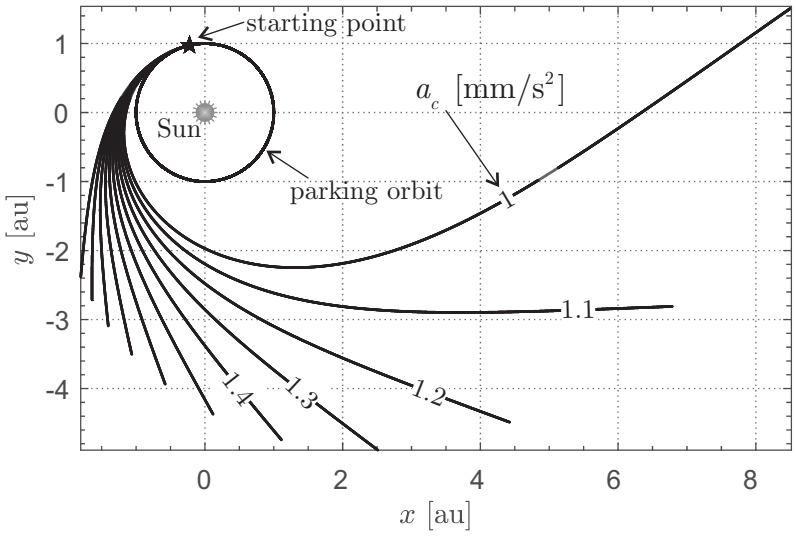

Figure 14. Near-optimal Solar System escape trajectories as a function of a_c for a circular parking orbit of radius $r_0 = 1$au.

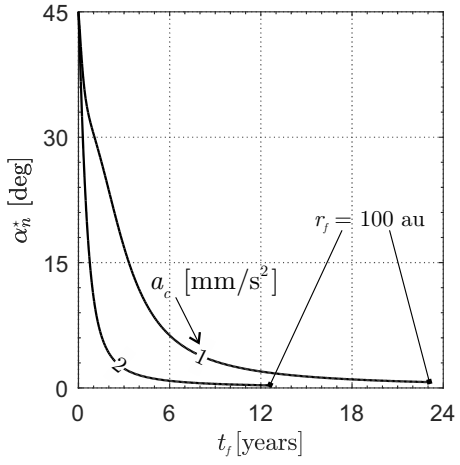

Figure 15. Locally-optimal steering law in a mission scenario with $a_c = \{1, 2\}$mm/s^2 and $r_f = 100$au.

gravity-assist maneuver nor any propellant consumption. The cranking phase provides an interesting scientific opportunity as it can be exploited for the analysis of the photosphere, the observation of solar poles, and the monitoring of solar activity. In this context, a deeper knowledge of the Sun would be useful to define a more refined E-sail thrust model, which takes into account the intrinsic variability of solar wind characteristics [10].

3.4. Rendezvous with Comet 67P/Churyumov-Gerasimenko

The European Rosetta mission was the first-ever space mission that successfully performed a cometary rendezvous with Comet 67P/Churyumov-Gerasimenko, a Jupiter-family comet, after a ten-year long transfer. For comparative purposes, the same target is studied using an E-sail-based spacecraft with $a_c = 1\,\mathrm{mm/s^2}$. The orbital elements of the comet [19] are reported in Tab. 2.

The locally-optimal control law linearly combines the time derivatives of a and i, thus obtaining a three dimensional transfer trajectory, whose ecliptic projection is shown in Fig. 17(a) together with a sketch of the

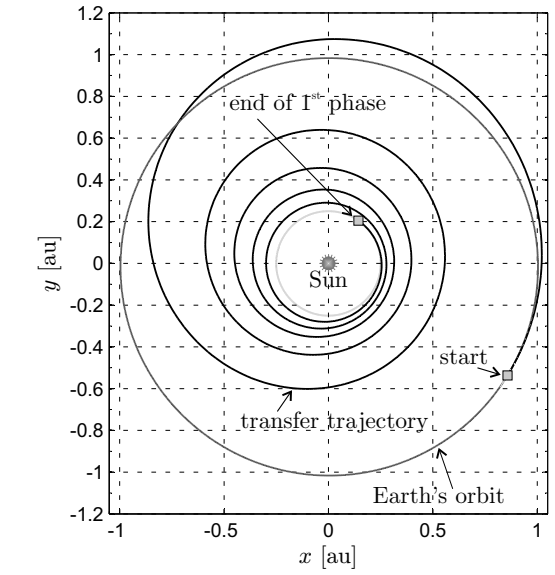

(a) First phase.

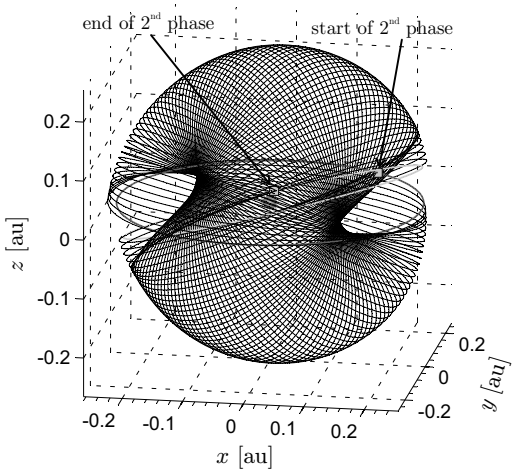

(b) Second phase.

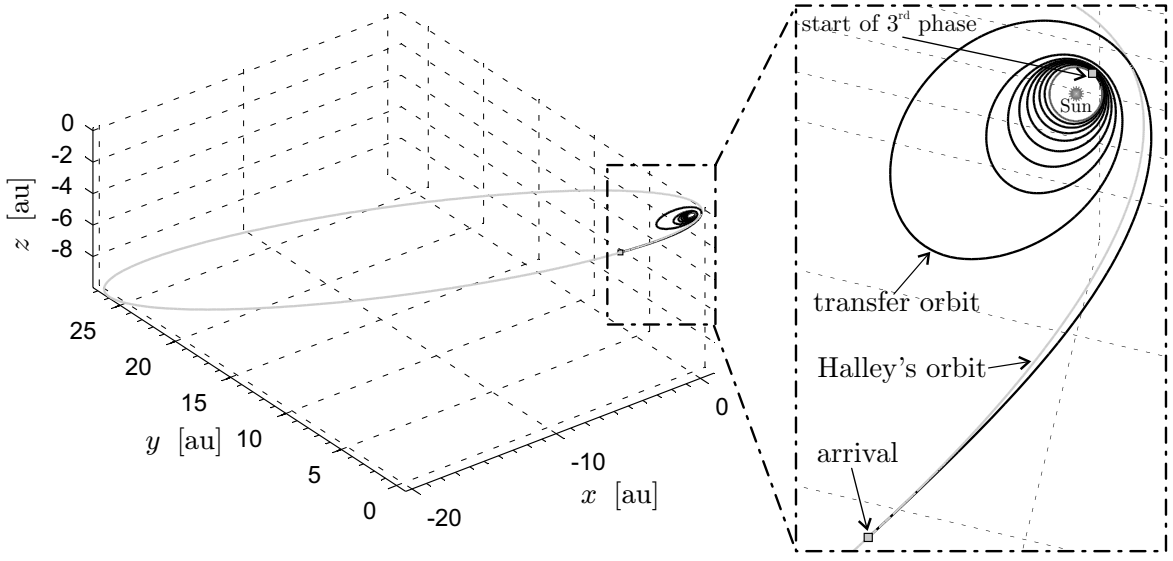

(c) Last phase.

Figure 16. Earth-Comet 1P/Halley locally-optimal transfer with $a_c = 1\text{mm/s}^2$.

E-sail thrust vector. The total flight time is about 2 years, a value considerably smaller than Rosetta's transfer time. Figure 17(b) illustrates the time variation of semimajor axis, eccentricity and inclination of the spacecraft osculating orbit, whereas Fig. 18 shows the locally-optimal steering law in terms of sail pitch $\alpha_n^\star$ and clock $\delta^\star$ angles.

These results can be compared with the globally-optimal values discussed in Ref. [20], and obtained with a less refined thrust model. Some similarities can be found between the two results, despite the two different optimization methods and E-sail acceleration models. The near-optimal solution yields a total flight time of 730 days, while the globally-optimal solution, which assumes a more effective thrust model, estimates a transfer duration of 340 days. In both cases of locally-optimal and globally-optimal control laws the cometary rendezvous

Orbital elements	Parking orbit	End of 1st phase	End of 2nd phase	End of 3rd phase
a [au]	1	0.2503	0.2504	17.83
e	0.0167	0.0010	0.0208	0.9671
i [deg]	0	0	162.26	162.26
ω [deg]	114.21	49.98	215.48	111.19
Ω [deg]	348.74	348.74	58.42	58.42
ν [deg]	225	16.32	231.74	138.18
t [years]	0	1.9820	11.1779	15.8567

Table 1. Orbital parameters for a comet Halley rendezvous with $a_c = 1\text{mm/s}^2$. Data adapted from Ref. [19].

a [au]	3.4630
e	0.6410
i [deg]	7.0405
ω [deg]	12.78
Ω [deg]	50.15

Table 2. Comet 67P/Churyumov-Gerasimenko orbital elements (referred to the 10^{th} of August 2014). Data adapted from Ref. [19].

occurs during the ascending phase. Also, the two transfer trajectories look like very similar even if the final orbital radii are quite different ($r_f = 2.69\,\text{au}$ for the globally-optimal solution and $r_f = 4.12\,\text{au}$ for the locally-optimal result).

4. Conclusions

A general approach for the study of locally-optimal control laws of an Electric Solar Wind Sail-based spacecraft has been discussed. The results are obtained by minimizing a linear combination of the time derivatives of the spacecraft osculating orbital elements. In general, the locally-optimal steering law must be calculated numerically by means of the simplex method. In some mission scenarios, however, when the control of a single orbital element is required, the locally-optimal solution can be obtained in an analytical form as a function of the spacecraft state variables. The proposed approach is simple to handle and requires a reduced computational cost. For example, in a cranking mission scenario, the locally-optimal approach is two order of magnitude faster than an indirect optimization method. The near-optimal results can be used as starting guesses for succeeding and more refined optimization algorithms. Different scientific mission scenarios have been discussed. The simulation results show the effectiveness of the proposed approach and its practical usefulness even in case of complex missions, where constraints on the spacecraft osculating orbital elements are introduced in order to satisfy the operational requirements of the propulsion system.

Declaration of conflicting interests

The authors declared no potential conflicts of interest with respect to the research, authorship, and publication of this article.

Funding

The authors received no financial support for the research, authorship, and publication of this article.

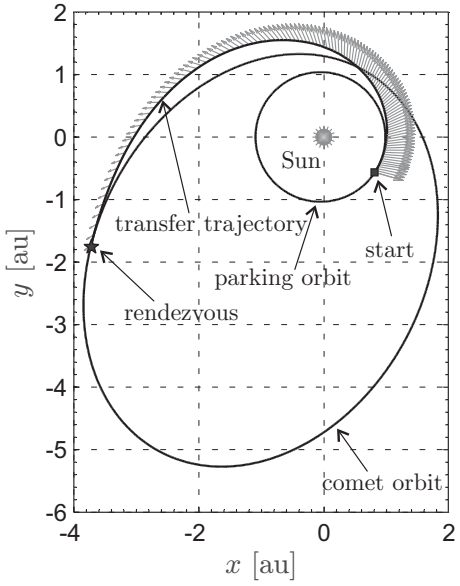

(a) Transfer trajectory (ecliptic projection).

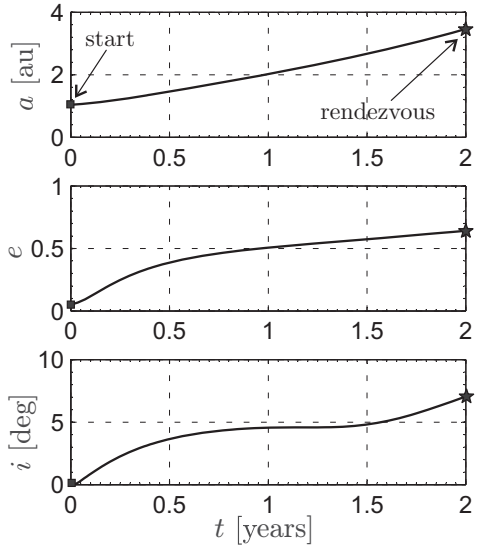

(b) Time variation of osculating orbital elements.

Figure 17. Earth-Comet 67P/Churyumov-Gerasimenko locally-optimal transfer with $a_c = 1\text{mm/s}^2$.

References

[1] Mengali G, Quarta AA. Tradeoff performance of hybrid low-thrust propulsion system. Journal of Spacecraft and Rockets. 2007 November-December;44(6):1263–1270.

[2] Mengali G, Quarta AA. Optimal Trade Studies of Interplanetary Electric Propulsion Missions. Acta Astronautica. 2008 June;62(12):657–667.

[3] Fu B, Sperber E, Eke F. Solar sail technology–A state of the art review. Progress in Aerospace Sciences. 2016 October;86:1–19.

[4] Macdonald M, McInnes CR, Dachwald B. Heliocentric solar sail orbit transfers with locally optimal control laws. Journal of Spacecraft and Rockets. 2007 January-February;44(1):273–276.

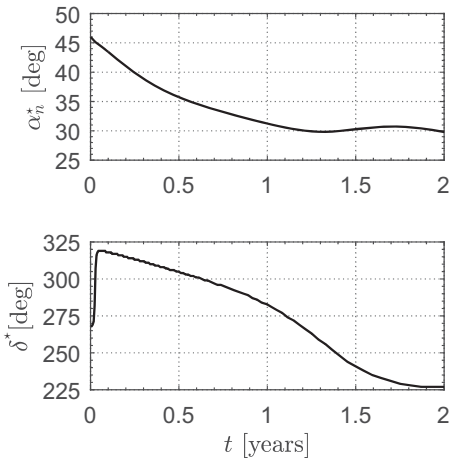

Figure 18. Time variation of the locally-optimal control law for Comet 67P/Churyumov-Gerasimenko rendezvous.

[5] Mengali G, Quarta AA, Janhunen P. Electric sail performance analysis. Journal of Spacecraft and Rockets. 2008 January-February;45(1):122–129.

[6] Huo M, Mengali G, Quarta AA. Optimal Planetary Rendezvous with an Electric Sail. Aircraft Engineering and Aerospace Technology. 2016;88(4):515–522.

[7] Quarta AA, Mengali G. Electric Sail Mission Analysis for Outer Solar System Exploration. Journal of Guidance, Control, and Dynamics. 2010 May;33(3):740–755.

[8] Yamaguchi K, Yamakawa H. Study on Orbital Maneuvers for Electric Sail with On-Off Thrust Control. Aerospace Technology Japan. 2013;12:79–88.

[9] Yamaguchi K, Yamakawa H. Electric Solar Wind Sail Kinetic Energy Impactor for Near Earth Asteroid Deflection Mission. The Journal of the Astronautical Sciences. 2016 March;63(1):1–22.

[10] Quarta AA, Mengali G. Minimum-Time Trajectories of Electric Sail with Advanced Thrust Model. Aerospace Science and Technology. 2016;55:419–430.

[11] Walker MJH, Ireland B, Owens J. A set of modified equinoctial orbit elements. Celestial Mechanics. 1985 August;36(4):409–419.

[12] Walker MJH. Erratum: a set of modified equinoctial orbit elements. Celestial Mechanics. 1986 April;38(4):391–392.

[13] Betts JT. Very Low-Thrust Trajectory Optimization Using a Direct SQP Method. Journal of Computational and Applied Mathematics. 2000 August;120(1):27–40.

[14] Battin RH. 10. In: An Introduction to the Mathematics and Methods of Astrodynamics, Revised Edition. Reston, Virginia: AIAA; 1999. p. 484–489. ISBN: 1-56347-342-9.

[15] Lagarias JC, Reeds JA, Wright MH, Wright PE. Convergence properties of the Nelder-Mead simplex method in low dimensions. SIAM Journal on Optimization. 1998 October–December;9(1):112–147.

[16] Heiligers J, McInnes CR. Solar sail heliocentric earth-following orbits. Journal of Guidance, Control and Dynamics. 2015 May;38(5):937–944.

[17] Lubin P. A roadmap to interstellar flight. JBIS: Journal of the British Interplanetary Society. 2016 February-March;69(2-3):40–72.

[18] Janhunen P. Electric Sail for Spacecraft Propulsion. Journal of Propulsion and Power. 2004 July-August;20(4):763–764.

[19] Zelenyi LM, Ksanfomality LV. From the Vega mission to comet Halley to the Rosetta mission to comet 67/P Churyumov-Gerasimenko. Solar System Research. 2016;50(7):451–463.

[20] Quarta AA, Mengali G, Janhunen P. Electric Sail Option for Cometary Rendezvous. Acta Astronautica. 2016 October-November;127:684–692.